THE EUROPEAN
PHYSICAL JOURNAL D

Regular Article

Shape and strength of dynamical couplings between vibrational levels of the H_2^+, HD^+ and D_2^+ molecular ions in collision with He as a buffer gas[⋆]

Ibrokhim Iskandarov[1], Francesco Antonio Gianturco[1,a], Mario Hernandez Vera[1], Roland Wester[1],
Humberto da Silva Jr.[2], and Olivier Dulieu[2]

[1] Institut für Ionen Physik und Angewandte Physik, Innsbruck Universität, Technikerstraße 25, 6020 Innsbruck, Austria
[2] Laboratoire Aimé Cotton, CNRS/Université Paris-Sud/ENS Cachan, Université Paris-Saclay, 91400 Orsay, France

Abstract. We present a detailed computational analysis for the interaction between the vibrating/rotating molecular ions H_2^+, HD^+, D_2^+ colliding with He atoms employed as buffer gas within ion trap experiments. The production and preparation of these molecular ions from their neutrals usually generate rovibrationally excited species which will therefore require internal energy cooling down to their ground vibrational levels for further experimental handling. In this work we describe the calculation of the full 3D interaction potentials and of the ionic vibrational levels needed to obtain the vibrational coupling potential matrix elements which are needed in the multichannel treatment of the rovibrationally inelastic collision dynamics. The general features of such coupling potential terms are discussed for their employment within a quantum dynamical modeling of the relaxation processes, as well as in connection with their dependence on the initial and final vibrational levels which are directly coupled by the present potentials. As a preliminary test of the potential effects on scattering observables, we perform calculations between H_2^+ and He atoms at the energies of an ion-trap by using either the rigid rotor (RR) approximation or the more accurate vibrationally averaged (VA) description for the $v = 0$ state of the target. Both schemes are described in detail in the present paper and the differences found in the scattering results are also analysed and discussed. We further present and briefly discuss some examples of state-to-state rovibrationally inelastic cross sections, involving the two lowest vibrational levels of the H_2^+ molecular target ion, as obtained from our time-independent multichannel quantum scattering code.

1 Introduction

Over the past 15 years or so, sympathetic cooling [1,2] has emerged as a versatile method for bringing a broad range of molecular ions down to milliKelvin secular temperatures. Sympathetic cooling relies on the simultaneous trapping of molecular ions with laser-cooled atomic ions. The ions exchange kinetic energy by elastic collisions which is removed by laser cooling of the atomic species. Due to the long range Coulomb interaction, the sympathetic cooling technique turns out to be efficient in the translational cooling while leaving the molecular ions internally hot [3,4].

Inelastic collisions with neutral buffer gas, however, have been repeatedly shown to represent an effective way to also cool the internal molecular degrees of freedom and of going beyond the translational cooling step [5]. This approach rests on the fact that in the framework of the neutral buffer gas cooling scheme, the rovibrational molecular temperature can be tuned to a value lower than the translational one, therefore useful for preparing a cloud of trapped molecular ions in a state of thermodynamic equilibrium.

A typical reaction scenario of a molecular ion AB^+ with He buffer gas, in which a broad variety of initial and final rovibrational levels can be involved, is given by:

$$AB^+(j,v) + \text{He} \rightarrow AB^+(j',v') + \text{He},$$
$$\text{where} \begin{cases} \text{rotational state } j > \text{ or } < j' \\ \text{vibrational state } v > \text{ or } < v'. \end{cases} \quad (1)$$
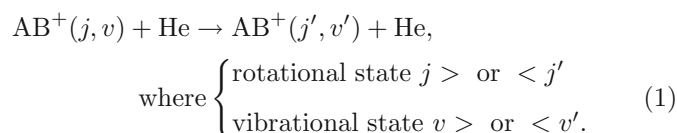
In order to estimate the relative efficiency of all the possible final channels for this reaction, one has to evaluate first the strength of the coupling between the rovibrational levels. Therefore, our preliminary analysis in this paper will focus on computing the vibrational coupling potentials between the vibrational levels of H_2^+, HD^+, D_2^+, in their electronic ground state, as induced by their interactions

with He atoms in the trap. To better illustrate the effect of our final potential coupling terms, we shall also briefly provide some quantitative results on state-to-state inelastic cross sections. It is also important to be reminded that the orientational anisotropy of such potential terms will also drive the rotational state-changing collisions and therefore will ultimately control the relative efficiency of the overall rovibrationally collisional cooling kinetics.

While the quantum physics of buffer gas cooling is of intrinsic interest as a benchmark problem in scattering theory, the species in our studies are the simplest of all one-electron molecules and can thus provide interesting data when employed as molecular targets in cold traps. Experiments involving these systems can also increase the accuracy of our evaluation of several existing fundamental constants, such as the Rydberg constant, nuclear radii and nucleus-to-electron mass ratios [6].

A relevant issue in the production of H_2^+ ion from neutral H_2 molecule is that H_2^+ ions formed from the impact of energetic electrons on H_2 will have several of its vibrational states populated according to a Franck-Condon distribution from the ionization processes of the ground-states of the initial neutral molecules. In illustrating this problem, Theard and Huntress [7] have shown that H_2^+ ions can be vibrationally de-excited in non-reactive encounters with helium and hydrogen gases, thereby lowering the population of the excited vibrational states for the ion in the trap. It is therefore at this stage of the molecular manipulation process that we need to have specific information on the structural features of the interaction potentials which would drive the internal cooling dynamics in the ion traps.

The paper is organized as follows: in Section 2, we outline the computational details involving the structure of the ground-state potential energy surfaces for H_2^+, HD^+, D_2^+ interacting with He atoms. We give there a brief summary of the computed vibrational states for the partner molecular ions. In Section 3, we study in detail the couplings between the various vibrational states of the systems and provide a brief summary of the formulae employed for the relevant vibrational couplings. In Section 4 we report some illustrative computational results on the excitation and de-excitation cross sections for the rotationally inelastic collisions when vibrational effects are incorporated. That same section also discusses a further illustrative example of the size and energy behaviour of the rovibrational cooling cross sections between the lowest two vibrational states of the H_2^+ molecular ion. All the scattering calculations reported in this section were performed using our in-house time-independent, multichannel quantum scattering code, as briefly discussed there. Finally, Section 5 presents our conclusions.

2 The computed interaction potentials between H_2^+, HD^+, D_2^+ and the He buffer gas

The interaction of H_2^+, HD^+ and D_2^+ with He atoms have been the subject of various investigations both experimentally [8] and theoretically [9], mainly involving studies

where the aim was to look at the proton transfer channel in the following reaction:

$$H_2^+ + He \rightarrow HeH^+ + H. \qquad (2)$$
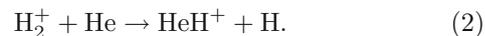
It had been shown earlier that this reaction is strongly endothermic [10] and can occur at low temperatures only when starting from vibrationally excited states of H_2^+. However, under the low-temperature conditions of the traps we intend to model, the molecular ions will be largely produced in their ground vibrational level thereby excluding any significant formation of the final products on the right-hand side of equation (2).

The processes we intend to study will then simply follow the scenario of equation (1), i.e. the collision physics of the trap partners will be controlled by the interaction potential for the internal-energy-transfer collisions without any significant chemical change. Such collisional channels will therefore evolve under a non-reactive anisotropic Potential Energy Surface (PES) which shall be the main object of the present study.

One of the earliest one-dimensional (1D) potential energy curve (PEC) calculations for the collinear geometry of H_2^+ with He had been performed by Edmiston et al. [11]. A more advanced study of the 2D surface including nonlinear geometries was constructed by Kuntz, where a semi-empirical diatomic-in-molecule (DIM) formalism was used to obtain the interaction potential [12]. Further calculations have been devoted to improve the level of accuracy of the surface and McLaughlin and Thompson were the first to perform truncated configuration interaction (CI) [13] studies. A mainly two-dimensional (2D) PES, with only a few angular "cuts" at different geometries of the partner molecular ion, was computed by Falcetta and Siska (F-S) who used an MCSCF MRCI level of quantum-chemical calculations with a $5s3p1d$ basis set for H and a $6s3p1d$ basis set for He [14]. More extensive calculations of the full 3D PES were carried out later on by Meuwly and Hutson (M&H) who employed the QCISD(T) level of quantum-chemical calculation and a correlation-consistent basis set expansion, the Dunning's aug-cc-pVQZ basis set [15]. Calculations of similar qualities were also carried out by Kraemer et al. [16] and Mrugala et al. [17] who employed a CASSCF approach with an active space consisting of four a′ and two a″ orbitals in order to obtain at the same time the ground and first excited electronic states of the system. The chosen basis set was $9s4p3d$ for He and $8s4p3d$ for H, contracted to $4s3p2d$ in each case. All the involved acronyms reported above are standard terminology within quantum chemical calculations so we refer the interested readers to the current, extensive literature on the subject.

A comparison of the well depth values obtained by the latest three independent calculations for the collinear geometry indicates that the values and locations of the well are very similar to each other, with relative differences of no more than a few percent [15]. A more detailed comparison of the most recent PESs will be discussed further below in relation with the present work.

The most recent PES employed for the system, and described in detail by [18], was obtained at very high

level of quantum chemical calculations, using the MRCI approach that included all single and double excitations from the initial CASSCF space. The calculated ab initio points were fitted using Aguado-Paniagua many-body expansion [19] in which the PES of the triatomic system ABC can be expressed as a sum of three monoatomic terms ($V_A^{(1)}$, $V_B^{(1)}$, $V_C^{(1)}$), three 2-body terms ($V_{AB}^{(2)}$, $V_{BC}^{(2)}$, $V_{AC}^{(2)}$) and one 3-body term $V_{ABC}^{(3)}$. The latter term is defined as:

$$V_{ABC}^{(3)}(R_{AB}, R_{AC}, R_{BC}) = \sum_{ijk}^{M} d_{ijk} \rho_{AB}^i \rho_{AC}^j \rho_{BC}^k, \quad (3)$$

where the optimal fitting was found by setting the parameter $M = 8$ for those geometries at FCI/cc-pVQZ level of theory, as further discussed in [19]. Here M is an order index of the expansion of a product function that decays exponentially with the distance and is defined in reference [18]. The detailed meaning of all terms has been given extensively in [18] and therefore will not be repeated here.

It is the latter choice for representing the relevant PES which we have employed in the present work. The data of [18] were provided by the authors as an interpolated potential function $V_{M8}(R_{H-H'}, R_{H-He}, R_{H'-He})$ which can be used for calculations related to the reaction reported by equation (2). Since the present work requires the use of Jacobi coordinates for the potential $V_{M8}(r, R, \theta)$, which are defined for the inelastic processes of interest in equation (1), we carried out the corresponding transformation of the PES of reference [18].

Thus, the vector $\mathbf{R}$, connecting the He atom and the molecular center of mass is simply

$$\mathbf{R} = \mathbf{x}_{He} - \frac{m_H \mathbf{x}_H + m'_H \mathbf{x}'_H}{m_H + m'_H}, \quad (4)$$

where, the H_2^+ interatomic distance is $R_{H-H'} = |\mathbf{r}| = |\mathbf{x}_H - \mathbf{x}'_H|$, with θ being the angle between $\mathbf{r}$ and $\mathbf{R}$. In the case when the two atomic masses are equal, the H_2^+ center of mass reduces to its midpoint,

$$\mathbf{R} = \mathbf{x}_{He} - \frac{1}{2}(\mathbf{x}_H + \mathbf{x}'_H). \quad (5)$$

The remaining two interatomic distances, R_{H-He} and $R_{H'-He}$, are readily given by geometric considerations,

$$\begin{cases} R_{H-He} = & \left\{ [x_H - R\cos(\theta)]^2 + [R\sin(\theta)]^2 \right\}^{1/2} \\ R_{H'-He} = & \left\{ [x'_H - R\cos(\theta)]^2 + [R\sin(\theta)]^2 \right\}^{1/2}. \end{cases} \quad (6)$$

Here, the variables given as "x" are the position vectors of each center with respect the origin of a space-fixed (SF) frame of reference.

One can easily extend the above coordinate transformation to the systems HD^+ and D_2^+ although the relation (4) will change for the case of HD^+, since H and D have different masses. The Fortran routine which produces
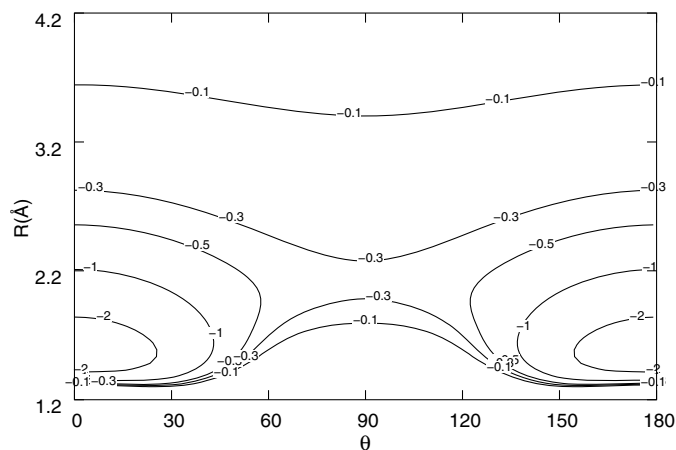
Fig. 1. Coutour plot of the PES $H_2^+ + He$ at the molecular bond length of $r = 1.0574$ Å. The attractive wells are located collinearly on both sides of H_2^+ target. Distances are in Å and energies in 10^3 cm^{-1}.

the 3D potential as a function of the Jacobi coordinates can be obtained on request from the present authors.

In Figure 1 the contour plot of H_2^+ interacting with He is given for the equilibrium geometry of the target molecular ion, where $\mathbf{r} = \mathbf{r}_{eq}$. The calculations have been performed for θ values from 0° up to 180° with 10° step size. As it can be clearly seen, there is still a markedly repulsive interaction when He comes along the 90° approach, while the two deepest wells of the potential correspond to the collinear geometries. It is also important to note here that the calculated potential for the case of a rigid rotor (RR), $V_{RR}(r_{eq}, R, \theta)$ is obtained at fixed equilibrium internuclear distance r_{eq} of H_2^+, just for the sake of providing a simpler example through the 2D cut of the full PES. In the general case, which is of interest to us in this work, of a vibrating molecular ion we shall of course obtain the full 3D PES as we shall discuss further below.

In order to better assess the overall quality of the general shape and strength of the presently chosen PES, we also compare some of its features with the earlier calculations of M&H [15] over three different values of the molecular bond distance which are within the range of the data presented by those authors. The comparison is given by the two panels of Figure 2: in the upper panel we show the radial cuts for the different values of the r-coordinate at the collinear approach, while the lower panel shows the same set of curves but for the case of the T-shape approach between partners.

There is a clear overall good agreement between the two sets of computed PESs: the two interaction potentials are essentially the same in terms of well depths for bond distances close to the equilibrium value. The fitting procedure of reference [15], in fact, produces small deviations for the stretched values, thereby enhancing the graphical differences.

In order to employ the presently obtained PES for non-reactive quantum scattering calculations, one has to further transform the PES in terms of the usual multipolar expansion. In other words, one has to first obtain
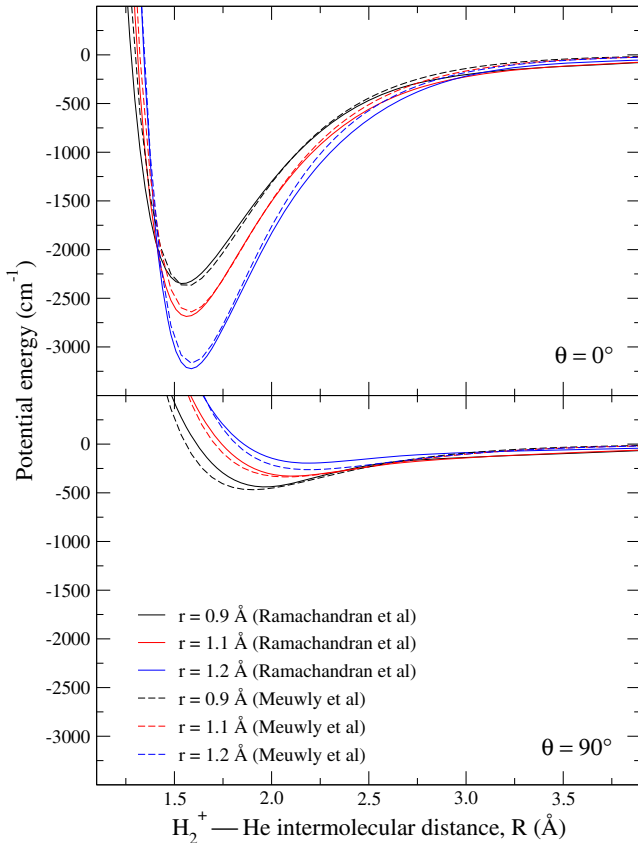
Fig. 2. Comparisons of the potential energy angular cuts for three different values of r from the two references reported in the main text.

the radial coefficients for the associated Legendre polynomial expansion of the original PES

$$V_{\text{tot}}(r, R, \theta) = \sum_{\lambda}^{\lambda_{\max}} V_{\lambda}^{\text{tot}}(r, R) P_{\lambda}(\cos \theta). \quad (7)$$

Here $V_{\lambda}^{\text{tot}}(r, R)$ are the radial terms of the multipolar expansion and $P_{\lambda}(\cos \theta)$ are the corresponding orthogonal Legendre polynomials. The above relation is written in a more general form which is considering the ionic target as a vibrating molecule. In the case where r is not anymore a variable but it is frozen at its equilibrium value, then we can simply obtain the 2D cuts of the full 3D PES and therefore write

$$V(r_{\text{eq}}, R, \theta) = \sum_{\lambda} V_{\lambda}(r_{\text{eq}}, R) P_{\lambda}(\cos \theta). \quad (8)$$

The last equation will be employed for the simpler problem of pure rotationally inelastic collisions which does not require generating vibrational coupling matrix elements. The Fortran routine for the multipolar expansion coefficients of above is also available on request from the authors.

In the following section we shall further discuss the 3D interaction potential required for the more general rovibrational state-changing processes.

Table 1. Energy of the $(J = 0)$ for three ionic targets (all energies in cm^{-1} units).

υ	H_2^+	HD^+	D_2^+
0	−21360.4649	−21513.8809	−21694.3128
1	−19166.8597	−19598.9225	−20115.9203
2	−17099.5771	−17779.1952	−18601.3592
3	−15154.9816	−16052.5722	−17149.6673
4	−13328.5964	−14416.2190	−15759.4384
5	−11616.2720	−12867.2238	−14429.0668
6	−10014.9248	−11403.0734	−13156.9649
7	−8522.8454	−10021.9328	−11941.7287
8	−7139.7106	−8722.7538	−10782.2440
9	−5866.4541	−7505.2709	−9677.7396
10	−4705.0997	−6369.9374	−8627.7994
11	−3658.6190	−5317.8438	−7632.3503
12	−2730.8414	−4350.6421	−6691.6362
13	−1926.4310	−3470.4883	−5806.1876
14	−1250.9501	−2680.0106	−4976.7934
15	−711.0455	−1982.3076	−4204.4767
16	−314.8538	−1380.9849	−3490.4778
17	−72.9222	−880.2429	−2836.2454
18	–	−485.0497	−2243.4363
19	–	−201.4771	−1713.9268
20	–	−37.4619	−1249.8377
21	–	–	−853.5789
22	–	–	−527.9251
23	–	–	−276.1460
24	–	–	−102.2553

2.1 Structure of the vibrational levels of H_2^+, HD^+ and D_2^+

We initially analyse the isolated $H_2^+(X^2\Sigma_g^+)$, $HD^+(X^2\Sigma^+)$ and $D_2^+(X^2\Sigma_g^+)$ potential energy curves for their ground electronic state. Such diatomic potentials are needed to obtain the corresponding wavefunctions and energies for their vibrational bound states of total angular momentum $J = 0$, i.e. for the non-rotating rigid rotor (RR) model of the isolated molecule. We shall not consider at this stage the splitting effects of both hyperfine structure and spin-rotation couplings that need to be considered in the full angular momentum coupling scheme for the open-shell target ions, as we have discussed in detail in a separate publication [20]. It was shown there that the sum of the individual state-to-state cross sections accounting for the fine-structure components is dynamically equivalent to directly treating the collision problem of a molecular ion as a structureless spherical rotor interacting with the He atom [20]. To generate the potential energy curves of the molecular ions, we have used exactly the same level of theory as it was done for $H_2^+ + He$ and we therefore refer the interested reader to the previous work for further details [18].

To obtain the vibrational wavefunctions a total of about 300 ab initio points were fitted to the individual sets of points corresponding in the potential routine to the asymptotic data for H_2^+ and HD^+, while for D_2^+ about 500 computed points were involved. In Table 1 the vibrational energy levels for the ground electronic states of $H_2^+(X^2\Sigma_g^+)$, $HD^+(X^2\Sigma^+)$ and $D_2^+(X^2\Sigma_g^+)$ are given

Table 2. A comparison between different calculated values for the first few vibrational levels of H_2^+, D_2^+ and HD^+, at $J = 0$, and those calculated in this work. The computed values were obtained using different approaches, some also accounting for relativistic and radiative corrections. Comparisons with experimental data are available in the respective references and the references reported therein. All energies are in wavenumbers in units of wavenumber with respect a selected reference energy at 0. The full references to the acronyms reported in the table are the following: JPK2006 [21]; LW1986 [22]; REM1989 [23]; REM1993 [24].

$v, J = 0$		H_2^+	D_2^+	HD^+	$v, J = 0$	H_2^+	D_2^+	HD^+
0	This work	−21360.46	−21694.31	−21513.88	4	−13328.60	−15759.44	−14416.22
	JPK2006	−21379.29	−21711.51	−21545.85		−13361.91	−15785.00	−14459.69
	LW1986	−21380.81	–	−21516.07		−13363.35	–	−14429.83
	REM1989	–	–	−21516.94		–	–	−14429.33
	REM1993	–	–	−21516.07		–	–	−14429.83
1	This work	−19166.86	−20115.92	−19598.92	5	−11616.27	−14429.07	−12867.22
	JPK2006	−19188.19	−20134.45	−19632.88		−11656.93	−14457.56	−12915.57
	LW1986	−19189.69	–	−19603.08		−11658.35	–	−12885.70
	REM1989	–	–	−19602.84		–	–	−12885.17
	REM1993	–	–	−19603.07		–	–	−12885.69
2	This work	−17099.56	−18601.36	−17779.19	6	−10014.92	−13156.96	−11403.07
	JPK2006	−17124.30	−18622.07	−17816.04		−10066.16	−13189.26	−11458.35
	LW1986	−17125.77	–	−17786.22		−10067.56	–	−11427.47
	REM1989	–	–	−17785.88		–	–	−11427.89
	REM1993	–	–	−17786.21		–	–	−11428.46
3	This work	−15154.98	−17149.67	−16052.57	7	−8522.84	−11941.73	−10021.93
	JPK2006	−15183.40	−17172.74	−16092.47		−8587.94	−11979.13	−10086.63
	LW1986	−15184.85	–	−16062.63		−8589.34	–	−10056.74
	REM1989	–	–	−16062.22		–	–	−10056.13
	REM1993	–	–	−16062.63		–	–	−10056.73

for the $J = 0$ rotational states. From the table we can see that the changes in masses and a small difference in the well depths of the potentials vary the number of vibrational states that they can support for the non-rotating molecular ions. Since D_2^+ is the heaviest molecule, for the range of computed points it exhibits 25 vibrational levels, while H_2^+ has only 18 and HD^+ 21.

We also present in Table 2 a comparison between the first few vibrational levels computed by us for the three systems and other computed values existing in the literature [21–24]. We can see from the data in the table that the agreement between our new calculations and the existing energy levels is rather good and confirms the overall quality of the present potential calculations.

The rovibrational wavefunctions will be obtained as products of each of the presently computed vibrational wavefunctions, from the states listed in Table 1, times the corresponding spherical harmonics describing the involved rotational state. Albeit a simplified picture, such partitioning has been used many times in the past and it is not expected to influence substantially the relevant physical processes. It is therefore this representation of the molecular rovibrational wavefunctions that will be employed in the calculations described in the following sections.

2.2 Vibrational couplings between H_2^+, HD^+ and D_2^+ ionic targets interacting with He atoms

We already saw from Figure 1 that a clear angular anisotropy exists for the PES of our system. We can further extend this analysis by varying the intramolecular
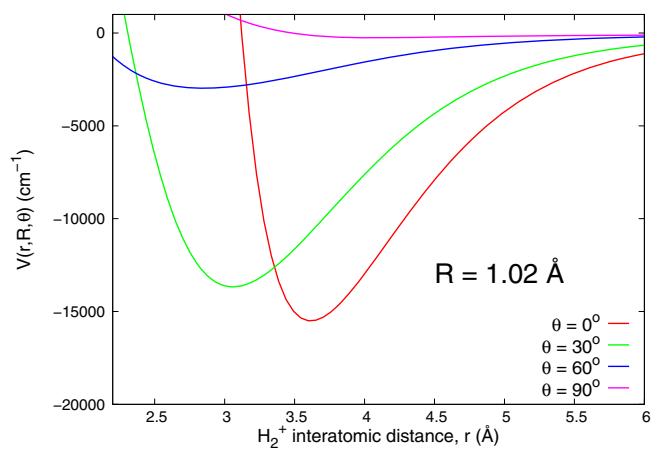
Fig. 3. Interaction potential as a function of the H_2^+ internuclear distance r for various angles θ. The value of R is kept fixed at one of the equilibrium geometry of the triatomic complex.

bond distance r which will then show how strongly r and R are coupled via the initial and final target's asymptotic vibrational states and through the presence of the impinging He atom. It will also show how their couplings vary with the orientational coordinate θ. For this purpose we have fixed R at the equilibrium geometry of the complex which occurs, following Figure 1, for $R = 1.02$ Å. Figure 3 therefore illustrates the dependence of the non-reactive interaction potential obtained in the present work on r for various angles and for a broad range of stretching values of the internal vibrational coordinate. As it could be expected, the overall potential appears to be less strongly influenced

by the H_2^+ geometry when $\theta = 90°$ while the variation is far more noticeable along the collinear approach on either of the hydrogen sides and as the projectile atom forms a stable complex with the molecular ion at the shown value of R. One should note here, in fact, that at the geometry of the complex triatomic system minimum energy configuration the couplings within the vibrating target states are expected to be significant at all angles, as we shall further illustrate below for different vibrational levels.

The crucial quantity of interest for carrying out the quantum dynamics is the coupling potential matrix between the various vibrational levels. The latter has its matrix elements defined as follows:

$$V_{v,v'}(R,\theta) = \int \phi_{v'}(r) V(r,R,\theta) \phi_v(r) dr. \qquad (9)$$

Each of the elements of the coupling matrix therefore describes the distortions of the vibrational states of the target ion by the interaction with the impinging He atom. If we consider now the full 3D multipolar expansion of the non-reactive PES the last relation can be rewritten within a similar expansion as the one of equation (6) before,

$$V_{v,v'}(R,\theta) = \sum_{\lambda} V_{v,v'}^{\lambda}(R) P_{\lambda}(\cos\theta). \qquad (10)$$

The spatial dependence of the coupling potentials for H_2^+ and HD^+ are respectively given in Figures 4 and 5. The Fortran routine which generates these matrix elements multipolar expansion coefficients can be obtained on requests from the authors.

We further show in Figure 4 the coupling potential matrix elements for D_2^+ (which are specified by the dashed lines). For H_2^+ and D_2^+ interacting with He, we are presenting examples only for two cases, collinear and perpendicular (T shape) geometries, although our actual calculations were done for the full range of angles reported by Figure 3. On the other hand, for the HD^+ target ion, given the reduced symmetry of this system, we are explicitly showing in Figure 5 three different angles of approach of the He partner.

As it can be seen from the figures, we have considered up to 8 vibrational levels when calculating the spatial features of the coupling potential matrix elements: they have been computed over the relevant range of atom-molecule radial distances within which the coupling potential is non-negligible. One sees from Figure 4 that the strongest vibrational coupling involves the approach on the H side where the lighter atom in the molecular ion is more easily affected by the perturbing He atom. Additionally the comparisons of the coupling potentials involving various vibrational states between H_2^+ and D_2^+, presented in detail by Figure 4, show that the strength of the coupling for H_2^+ case is uniformly stronger. This fact could be explained as due to the mass differences between H and D since the heavier isotope generates a higher density of vibrational levels that are more closely spaced than in the case for the lighter molecular ion. The corresponding coupling matrix elements will therefore be smaller.
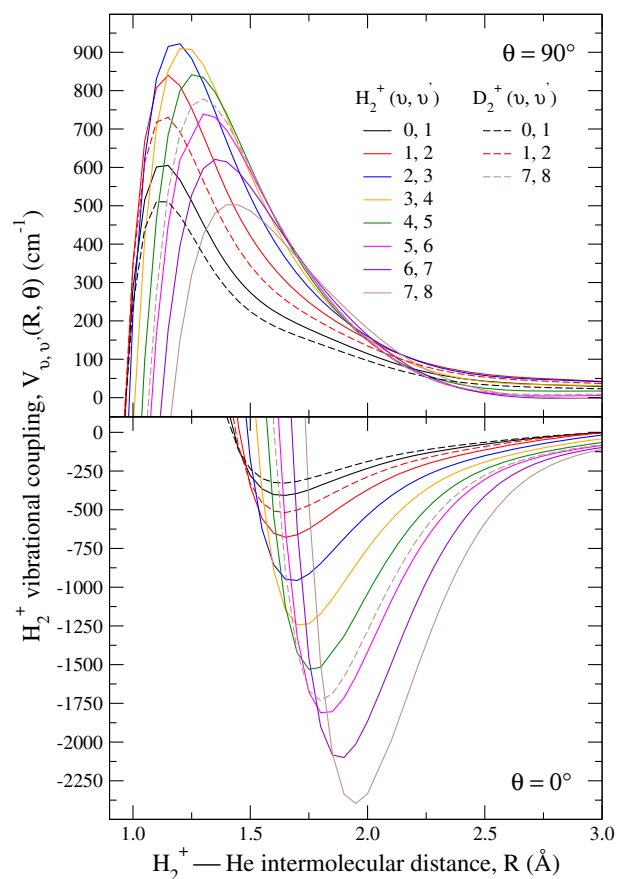
Fig. 4. Computed off-diagonal matrix elements from equation (9) as a function of R and for two values of the angle θ for H_2^+ and D_2^+. The plot on the top shows the T shape while the bottom one is for collinear geometries.

As already discussed earlier, the anisotropy of the present interaction potentials affects the magnitude of the vibrational coupling matrix elements as one varies the angle of approach between partners. More specifically, the radial coefficients generated by the multipolar expansions of equation (9) will show different strength and different radial range of their coupling values as the anisotropy index λ is changed.

Since our present task is to analyse the collisional dynamics of the complexes, it is instructive to see the behaviour of those multipolar coefficients, $V_{v,v'}^{\lambda}(R)$, as a function of R and for various vibrational states present in the off-diagonal elements of that coupling matrix.

In Figures 6 and 7 we present the computed $V_{v,v'}^{\lambda}(R)$ for H_2^+ and HD^+ respectively. In Figure 6, we present several panels corresponding to the lower values of $\lambda = 0, 2, 4, 6$, showing the $V_{v,v'}^{\lambda}(R)$ couplings between several off-diagonal indices involving the lower vibrational states as labelled in that figure. Additionally, in one of the panels (for $\lambda = 2$) in Figure 6, the $V_{v,v'}^{\lambda}(R)$ for the heavier isotopic variant D_2^+ are given.

For the case of the polar ion HD^+ we present in Figure 7 the $V_{v,v'}^{\lambda}(R)$ coupling coefficients for a series of values involving $\lambda = 0, 1, 2, 3$: we are covering the same range
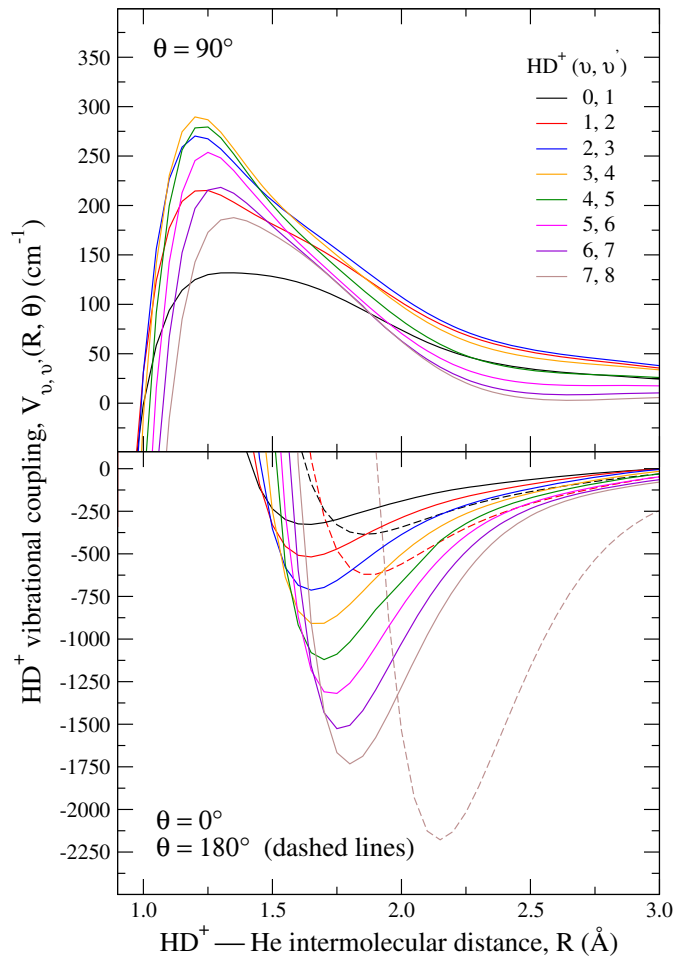
Fig. 5. Computed off-diagonal matrix elements from equation (9) for the case of the HD^+ molecular ion, as a function of R and for three values of the angle θ. The plot on the top shows the T shape while the bottom one is for collinear geometries. The latter curves are given by thicker lines.

of vibrational states as in Figure 6. One sees from a comparison with similar data in Figure 6 that the $\lambda = 2$ involves the strongest coupling, which maintains a marked strength over the whole radial range presented. Furthermore it is the odd values of λ which now are as strong as those which are even in Figure 6. Additionally, the couplings between the higher vibrational states show reduced strength in comparison with the even values of the λ multipolar coefficients.

3 Effects from vibrational averaging: the $v = 0$ case

One of the common approximations for the calculations of rotationally state-changing cross sections within the ground vibrational levels of a diatomic molecule, neutral or ionic, is to employ the rigid rotor (RR) approximation where the internuclear distance is kept fixed during the process at its $r = r_{eq}$ value. The more general case is of course, the one where r is no longer kept fixed and there-
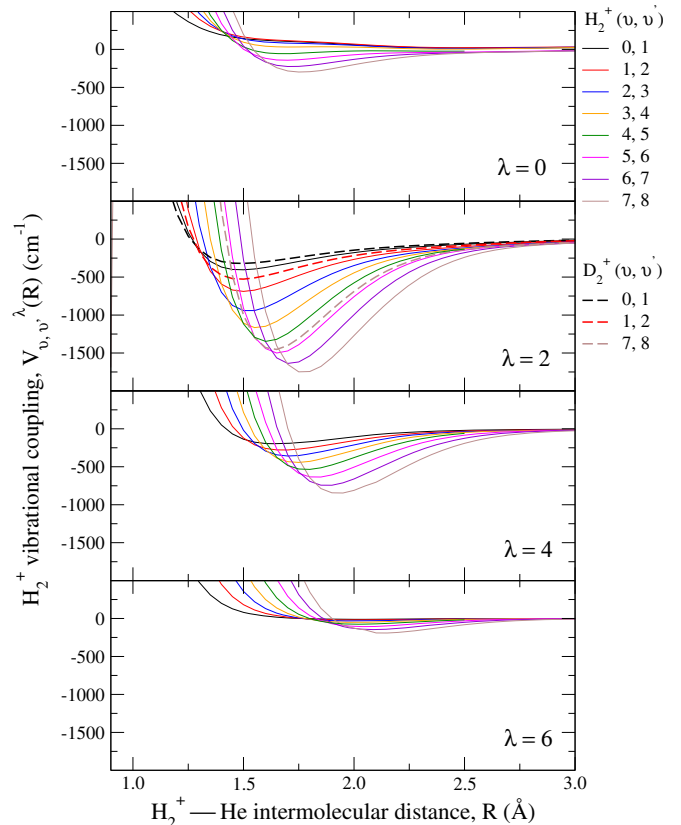
Fig. 6. Some of the computed multipolar expansion coefficients for the matrix elements $V_{v,v'}^\lambda(R)$ as a function of R for H_2^+ (solid lines) and D_2^+ (dashed lines) with $\lambda = 0, 2, 4, 6$.

fore the rotationally inelastic cross sections are computed via a more realistic description of the vibrational motion of the target molecule, especially when excited vibrational states are involved as in the present study. This also holds when the target ion is kept in its ground vibrational state during the rotationally inelastic processes.

In this section we shall therefore analyse the implications from using a more extended coupling potential for the exemplary case of the H_2^+ molecular ion. The results can be extended to the other molecular ions following the same approach.

The potential of a rigid rotor can be written as

$$V_{RR}(R,\theta) = \int \delta(r - r_{eq})V(r, R, \theta)dr. \qquad (11)$$

Here $\delta(r - r_{eq})$ is a Dirac's delta function which basically plays the role of a symmetric vibrational wavefunction centered around the $r = r_{eq}$ value of the target molecule: for this specific case the wavefunction is obviously only a sharp peak around that value. It physically describes schematically a highly harmonic oscillator for the $v = 0$ state. We shall call this approximation the HO-RR scheme for including vibrational effects.

On the other hand, the PES of the full 3D potential where r is a variable should be written as in equation (9), which we repeat below for the special case of the ground
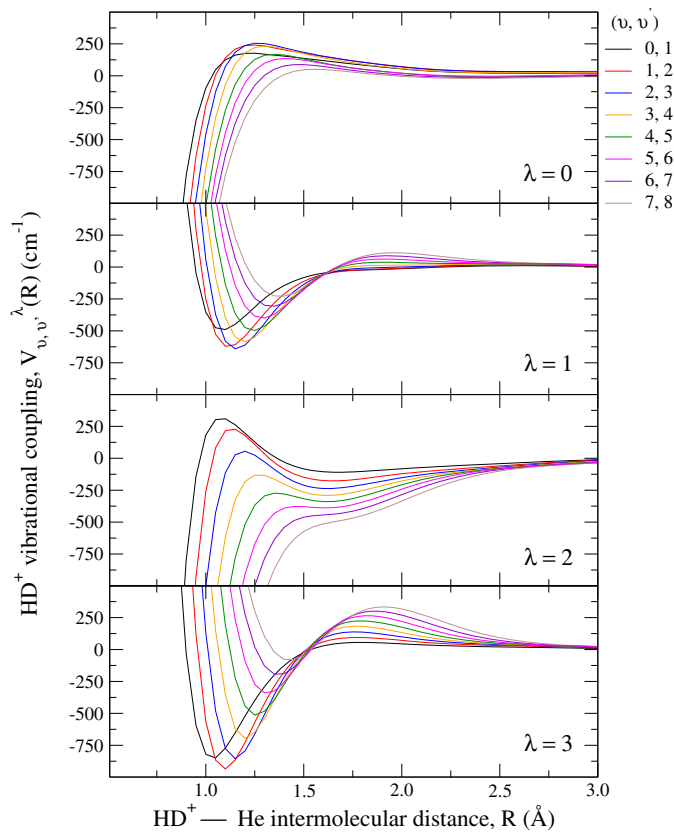
Fig. 7. Computed multipolar expansion coefficients for the coupling matrix elements $V_{v,v'}^{\lambda}(R)$ as a function of R for HD$^+$ with $\lambda = 0, 1, 2, 3$.

Fig. 8. Different "cuts" of the PES for the H$_2^+$-He system computed at different orientation angles. Solid lines: HO-RR potential; dashed lines: VA potential for the $v = 0$ case.
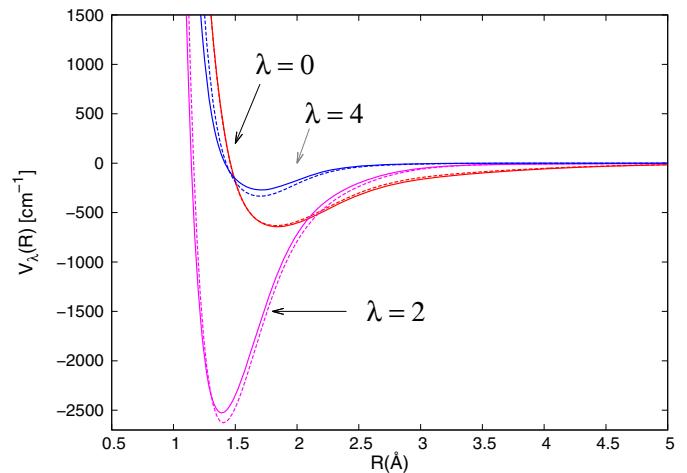
Fig. 9. Radial dependence of the corresponding multipolar expansion V_λ coefficients of H$_2^+$-He complex computed for different values of the index λ. The solid and the dashed lines have the same meaning as in the previous figure.

vibrational wavefunction of the molecular partner:

$$V_{\mathrm{VA}}(R, \theta) = \int \psi_{v=0}(r) V(r, R, \theta) \psi_{v=0}(r) dr. \qquad (12)$$

In this case the PES is averaged over the physical ground state vibrational wavefunction and the resultant interaction scheme is here called the vibration-averaged (VA) potential scheme. To provide specific examples of its behaviour, we present in Figure 8 several angular cuts of the computed PES for the H$_2^+$-He following equation (12). For completeness we have also shown in Figure 9 the dependence of the various multipolar coefficients V_λ on the radial atom-molecule variable R.

In the figures we have compared the (HO-RR) and (VA) potential schemes, the latter obtained for the $v = 0$ level of the lightest homonuclear ion. They also give an overview of the angular anisotropy and the strength of the potential coupling for the ground vibrational state of the targets.

By looking at the locations of the well depth as a function of the chosen angles, as it was already discussed in an earlier section, we can see that the collinear cases exhibit the deepest wells while the bent approaches show weaker interactions: the well depths decrease down to more than 90% from the collinear value. It is also evident that the (VA) potential shows a coupling strength around the potential well which is slightly stronger than (HO-RR). This

means that even in the ground vibrational level the target ions present a small, but visible anharmonicity to affect the interaction potential, which will in turn generate the rotationally inelastic cross sections as we shall further discuss later.

4 HO-RR and VA rovibrational state-changing cross sections

To calculate the relative inelastic cross sections we used the quantum Coupled-Channel (CC) method for solving the scattering equations, employing an in-house developed scattering code: the ASPIN code [25]. Since that code has been presented and discussed many times before, we shall omit the details of its numerical implementation of the well-known CC approach. Suffices it to say that the number of closed rotational channels needed to be included
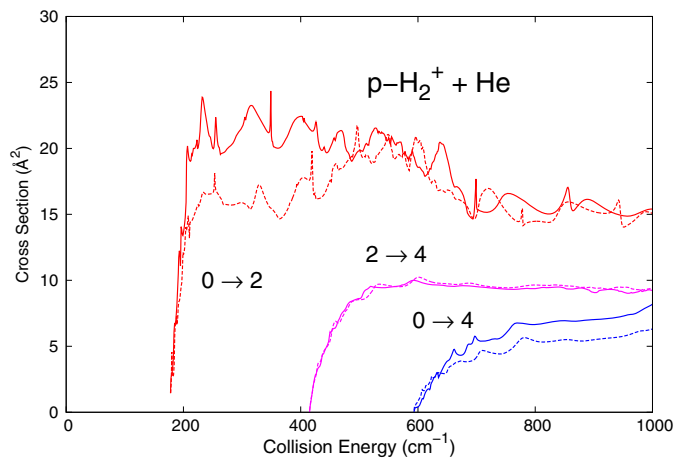
Fig. 10. Computed cross sections as a function of collision energy for transitions from the lowest to various rotational excited rotational states of para-H_2^+. The solid lines report the OH-RR scheme calculations, while the dashes describe the results obtained by the VA method for generating the coupling potential in the ground vibrational levels of the molecular targets.
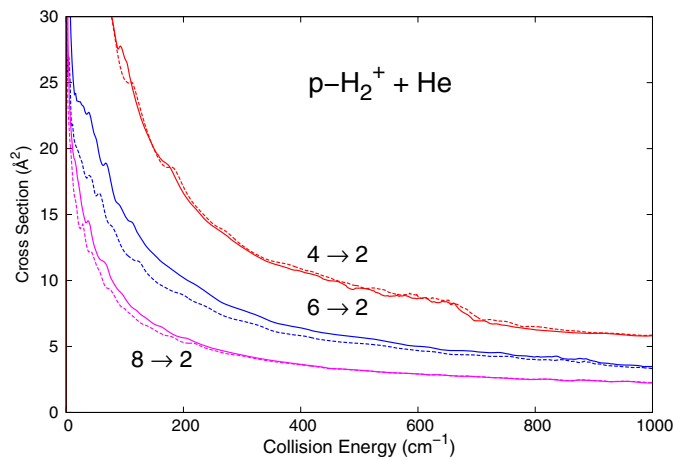
Fig. 11. Computed cross sections as a function of collision energy for various transitions to lower rotational states and starting from different initial rotational levels of para-H_2^+.

in the multichannel expansion in order to achieve a 2% accuracy in the numerical convergence of the individual cross sections turned out to be four.

The inelastic cross sections that we are interested in correspond to the state-changing processes for the target ion H_2^+ in an initially excited rotational state and we shall initially keep the vibrational state fixed at $v = 0$ during the collisional events.

In Figures 10 and 11, the excitation and de-excitation cross sections are given as a function of collisional energy for various pure rotational transitions. The dashed and solid lines correspond to the same transitions but using either the (HO-RR) or the (VA) potentials respectively. From Figure 10 it can be seen that the largest excitation cross section corresponds to the transition from $j = 0$ to $j = 2$ rotational states which is nearly a factor of

four larger than all the others. Thus, this transition is markedly favored since it is directly linked to the corresponding strength of the anisotropic coefficient for $\lambda = 2$, as shown in Figure 9.

The calculations of the de-excitation cross sections reported by Figure 11 cover the same energy range, already discussed in Figure 10. One sees there the H_2^+ ions, having been prepared in one of the lowest three rotational states, are collisionally cooled down to the $j = 2$ rotational level as a specific example of the collisional process. It is evident from Figure 11 that the cross sections exhibit similar behaviour, in the sense that they markedly increase as the temperature decreases. One further sees that the de-excitation cross sections strength markedly depends on the energy gaps involved. Thus, the quenching of the ions turns out to be most efficient when the de-excitation dynamics is chiefly controlled by the $\lambda = 2$ anisotropic coefficient of the interaction potential. We can also see that the treating of the potential either as a rigid rotor or by taking its vibrational average (VA scheme) affects the final cross sections mainly in the lowest range of collision energies: the anharmonicity becomes therefore more significant when the collision energies approach their relative thresholds. The excitation process for the $0 \rightarrow 2$ transition shows the largest difference between the two different schemes for generating the coupling potentials discussed above at energies very close to threshold (see Fig. 10).

We only discuss in the present work the general features and relative behaviour of the rotationally inelastic cross sections since we intend to chiefly focus our presentation on the features of the full interaction potential that we have obtained from the present calculations. A more extended discussion of the variety of inelastic cross sections in the low temperature region which we have obtained for the present systems has been presented in a separate publications [20,26]. We therefore refer the interested reader to it for further details.

As mentioned in the introduction, the present analysis of the shape and strength of the vibrational coupling potential matrix elements is ultimately directed to the calculation of inelastic processes involving state-changing rovibrational collisions.

To briefly illustrate the behaviour of some specific examples involving rovibrational heating and cooling cross sections, we report some of the relevant cross sections (identified by two-number labels) in Figures 12 and 13. The first label indicates the initial vibrational state and the second specifies the initial rotational state within the chosen vibrational level, respectively. The numerical convergence tests have been carried out by including up to four closed rotational levels and up to two closed vibrational levels, as described for our in-house computer coding in a separate publication [25].

We can clearly see that the order of magnitude of the cross sections, for cases where the collision dynamics vibrationally cools but rotationally excites the target ion (Fig. 13), follows a similar strength-ordering as that shown by the pure rotational de-excitation processes (see Figs. 10 and 11). On the other hand, the opposite
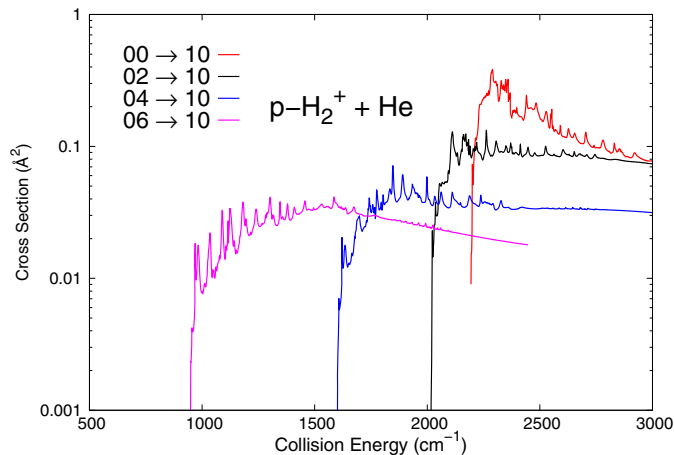
Fig. 12. Computed cross sections as a function of collision energy for various transitions from rotationally excited ($j = 0, 2, 4, 6$) levels of para-H_2^+, in its ground vibrational level ($v = 0$) to a vibrationally excited ($v = 1$) molecular partner in its $j = 0$ rotational level.
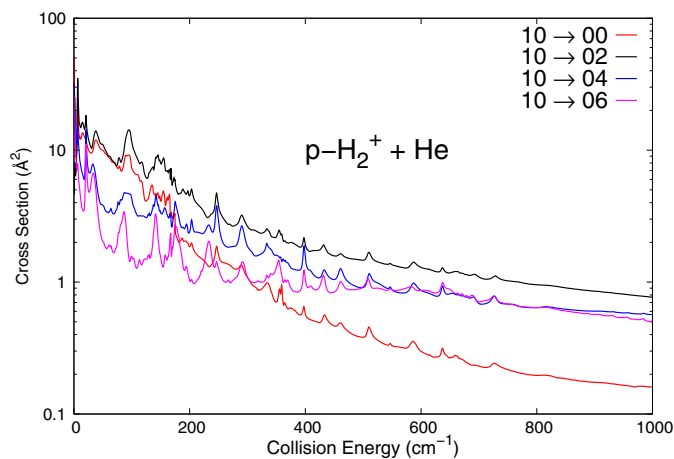
Fig. 13. Computed cross sections as a function of collision energy for various transitions to lower vibrational states, of para-H_2^+, producing rotationally excited molecular ions ($j = 0, 2, 4, 6$).

happens when one looks at the excitation rovibrational channels reported by Figure 13: starting with target molecular ions which are already rovibrationally excited produces cross sections which are around one order of magnitude smaller than those for the channel where only vibrational excitation occurs. This indicates that the pure vibrational excitation probability, albeit smaller than the rotational excitation probability seen before, is the most efficient excitation process within the rovibrational manifold. A more detailed and extensive analysis of a larger range of rovibrational processes will be presented elsewhere and is being prepared for a future publication. We provide here a brief analysis of their features to demonstrate that the present full interaction potential can indeed yield meaningful results for the state-to-state quantum energy transfer probabilities: the latter will be more extensively discussed elsewhere.

5 Conclusions

In this work we have analyzed in some detail the full three-dimensional interaction of H_2^+, HD^+ and D_2^+ with He atoms by computationally exploring the strength and radial range of the coupling potential matrix elements between the various vibrational levels in their ground electronic states. In order to realize this, first the potential energy surfaces of the ions have been obtained earlier [18], by using accurate ab initio methods and covering the full range of the 3D space configuration. In the next step we have fitted the obtained ab initio points with an accurate high-level many-body expansion in Jacobi coordinates and have then computed the corresponding asymptotic, isolated wavefunctions of all the vibrational states of H_2^+, HD^+ and D_2^+ by using the same level of theory used in [18] to obtain the required PEC of each diatom. We have also provided some illustrative examples for the state-to-state rovibrationally inelastic cross sections obtained from our own multichannel quantum computing code [25] and have briefly discussed their relative size and energy dependence.

Since the previous studies on the production of these molecular ions in traps containing He atoms [7] indicated the first 6 to 8 vibrational levels to be most abundantly present, we have focussed on the first eight vibrational levels in each molecular ion and have additionally computed the full 3D PES of the H_2^+ − He complex. When examining the 2D cuts of the PES where the target ions were kept at their equilibrium geometries, we have further found that the collinear approaches provide the stronger interaction with respect to the bent approaches of the impinging He atom. This behaviour turned out to be true when we have analysed the V_λ couplings between the various vibrational states for both H_2^+, D_2^+ and HD^+ at different orientations. We have also generated the corresponding multipolar coefficients that measure the overall anisotropy of the interaction between partners. As mentioned earlier in this paper, all the Fortran routines that we have obtained to describe the interaction potential are available on request from the authors.

In order to further provide specific examples of the effects from the potential features on different scattering observables, we have initially looked at the role of the averaged potential over the ground vibrational states and compared it with the case of a rigid rotor scheme that provides a simpler coupling potential. We then found that the vibrationally averaged (VA) potential scheme provided small but significant differences in the potential shape with respect to the HO-RR potential.

The effects on the final cross sections from using the VA potential scheme have been analysed via the calculations of the collisional excitation and de-excitation between pure rotational levels for H_2^+. We found that this effect is fairly small, although it gets more marked when the collisional energies are close to the corresponding thresholds.

As an additional example of the effects on scattering observables from the vibrational coupling matrix elements, we have shown preliminary results involving the use of the (2×2) vibrational matrix for the lowest

two vibrational levels and computed with it the rovibrational heating and cooling cross sections at the same energies of the purely rotationally inelastic processes. We found that pure vibrational excitation cross sections are the largest within the manifold, although in general the opening of vibrational levels strongly reduces the efficiency of the energy transfer dynamics in comparison with the pure rotationally inelastic channels.

In conclusion our present work has provided detailed information on the structural features of a specific set of interaction potentials involving He atoms and hydrogen molecular ions. Such information will be used in a later work for a more extensive analysis of the relative efficiency of the rovibrational excitation and de-excitation of a broad range of collisional channels. The latter will be those involved in the cooling dynamics of the present molecular ions by He as the buffer gas under trap conditions.

Author contribution statement

All authors have contributed equivalently to different aspects and stages of the overall research project described in the present work.

References

1. R. Wester, J. Phys. B **42**, 154001 (2009)
2. K. Ravi, S. Lee, A. Sharma, G. Werth, S.A. Rangwala, Nat. Commun. **3**, 1126 (2012)
3. A. Bertelsen, S. Jørgensen, M. Drewsen, J. Phys. B **39**, L83 (2006)
4. K. Okada, M. Wada, T. Takayanagi, S. Ohtani, H.A. Schuessler, Phys. Rev. A **81**, 013420 (2010)
5. A.K. Hansen, O.O. Versolato, L. Kłosowski, S.B. Kristensen, A. Gingell, M. Schwarz, A. Winderberger, J. Ullrich, J.R. Crespo López-Urrutia, M. Drewsen, Nat. Lett. **508**, 76 (2014)
6. P.J. Mohr, B.N. Taylor, D.B. Newell, J. Phys. Chem. Ref. Data **41**, 043109 (2012)
7. L.P. Theard, W.T. Huntress Jr., J. Chem. Phys. **60**, 2840 (1974)
8. F.S. Klein, L. Friedman, J. Chem. Phys. **41**, 1789 (1964)
9. P.J. Brown, E.F. Hayes, J. Chem. Phys. **55**, 922 (1971)
10. S. Bovino, M. Tacconi, F.A. Gianturco, J. Phys. Chem. A **115**, 8197 (2011)
11. C. Edmiston, J. Doolittle, K. Murphy, K.C. Tang, W. Wilson, J. Chem. Phys. **52**, 3419 (1970)
12. P.J. Kuntz, Chem. Phys. Lett. **16**, 581 (1972)
13. D.R. McLaughlin, D.L. Thompson, J. Chem. Phys. **70**, 2748 (1979)
14. M.F. Falcetta, P.E. Siska, Mol. Phys. **88**, 647 (1996)
15. M. Meuwly, J.M. Hudson, J. Chem. Phys. **110**, 3418 (1999)
16. W.P. Kraemer, V. Spirko, O. Bludsky, Chem. Phys. **276**, 225 (2002)
17. F. Mrugala, V. Spirko, W.P. Kraemer, J. Chem. Phys. **118**, 10547 (2003)
18. C.N. Ramachandran, D. De Fazio, S. Cavalli, F. Tarantelli, V. Aquilanti, Chem. Phys. Lett. **469**, 26 (2009)
19. A. Aguado, C. Tablero, M. Paniagua, Comput. Phys. Commun. **108**, 259 (1998)
20. M. Hernández-Vera, F.A. Gianturco, R. Wester, H. da Silva Jr., O. Dulieu, S. Schiller, J. Chem. Phys. **146**, 124310 (2017)
21. J.Ph. Karr, L. Hilico, J. Phys. B **39**, 2095 (2006)
22. L. Wolniewicz, J.D. Poll, Mol. Phys. **59**, 953 (1986)
23. R.E. Moss, I.A. Sadler, Mol. Phys. **66**, 591 (1989)
24. R.E. Moss, Mol. Phys. **78**, 371 (1993)
25. D. López-Durán, E. Bodo, F.A. Gianturco, Comput. Phys. Commun. **179**, 821 (2008)
26. M. Hernández Vera, S. Schiller, R. Wester, F.A. Gianturco, Eur. Phys. J. D **71**, 106 (2017)
27. A. Sen, J.W. McGowan, J.B.A. Mitchell, J. Phys. B **20**, 1509 (1987)